JOURNAL OF GEOPHYSICAL RESEARCH, VOL. 103, NO. A11, PAGES 26,559–26,572, NOVEMBER 1, 1998

Small-scale, dispersive field line resonances in the hot magnetospheric plasma

A. V. Streltsov and W. Lotko
Thayer School of Engineering, Dartmouth College, Hanover, New Hampshire

J. R. Johnson and C. Z. Cheng
Plasma Physics Laboratory, Princeton University, Princeton, New Jersey

Abstract. The formation, temporal behavior, and spatial structure of field line resonance (FLR) layers formed by shear Alfvén waves standing along auroral magnetic field lines between the ionospheres are investigated when the layer develops transverse structure on the scale of the ion Larmour radius. Using a new numerical model including full ion Larmour radius correction in dipole magnetic geometry with realistic distributions of background plasma temperature and density, the following is shown: (1) Hot magnetospheric ions significantly retard the development of a parallel electric field in ion gyroscale dispersive Alfvén waves. (2) A fundamental FLR forming near $L = 7.5$ can contract to a transverse scale size of several hundred of meters in the direction perpendicular to the geomagnetic field at ionospheric altitudes, with a parallel electric field sufficient to produce a kV potential drop along the resonance field line from the ionosphere up to $\sim 4\ R_E$ altitude, in the region where the wave dispersion is due to the finite electron inertia. (3) A plasma density depletion in the lower auroral magnetosphere ($\approx$ 2–5 R_E geocentric distance) enables the formation of a nonradiative fundamental FLR. (4) Dispersive FLRs for the higher harmonics are more radiative at the equatorial magnetosphere than the fundamental mode.

1. Introduction

Many theoretical studies of dispersive Alfvén waves in the space plasma have been performed since the seminal studies by *Hasegawa* [1976] and *Goertz and Boswell* [1979] showed that these waves have a component of the electric field parallel to ambient magnetic field lines sufficient to accelerate electrons into the ionosphere. This feature of dispersive Alfvén waves suggests that they may be responsible for some classes of auroral arcs, produced by sheet-like fluxes of precipitating electrons with energies from 100 eV up to tens of keV [*Swift*, 1975; *Davis*, 1978; *McFadden et al.*, 1986; *Boehm et al.*, 1990; *Samson et al.*, 1991], and a number of such models have been developed [*Hasegawa*, 1976; *Mallinckrodt and Carlson*, 1978; *Lysak and Dum*, 1983; *Haerendel*, 1983; *Goertz*, 1984; *Temerin et al.*, 1986; *Chmyrev et al.*, 1988; *Seyler*, 1990; *Hui and Seyler*, 1992; *Samson et al.*, 1992; *Kletzing*, 1994; *Wei et al.*, 1994; *Trondsen et al.*, 1997].

In spite of considerable theoretical efforts in recent years to connect dispersive shear Alfvén waves to the formation of discrete auroral arcs at subkilometer scales transverse to the magnetic field two fundamental questions remain [*Borovsky*, 1993]. (1) How are shear Alfvén waves generated on auroral field lines? (2) How do these waves contract to transverse scales sufficiently small to produce subkilometer scale arcs? Of related interest are the conditions that allow Alfvén waves with a period in the range of 10–500 s to produce extremely narrow and intense electric fields and currents, less than 1 km wide in the north-south direction and extended up to 1000 km in the east-west direction (referenced to the ionospheric height).

Intense, transversely localized fields are frequently measured on polar-orbiting satellites [*Kletzing et al.*, 1983; *Dubinin et al.*, 1985; *Chmyrev et al.*, 1988; *Weimer and Gurnett*, 1993; *Marklund et al.*, 1995; *Mishin and Förster*, 1995; *Aikio et al.*, 1995; *Karlsson and Marklund*, 1996] and rockets [*Boehm et al.*, 1990] and are thought to be the lower magnetospheric signatures of auroral arcs and black aurora. Because the periods of ULF Alfvén waves are compatible with fundamental field line oscillations and the timescale of particle bounce motion along auroral field lines, their behavior can be an important indicator of the plasma parameters and electromagnetic activity of the magnetosphere along the entire magnetic flux tube. Therefore quantitative modeling of processes leading to generation of dispersive Alfvén waves in the magnetosphere, including their propagation through strongly inhomogeneous me-

Copyright 1998 by the American Geophysical Union.

Paper number 98JA02679.
0148-0227/98/98JA-02679$09.00

dia, interaction with the ionosphere, and ability to accelerate particles, is important for understanding a variety of problems associated with magnetosphere-ionosphere coupling.

One mechanism for exciting a shear Alfvén wave in the magnetosphere involves mode coupling between the shear mode and an externally driven, large-scale MHD surface wave, which is a localized incompressible mode in a plasma with an isolated transverse gradient of the background Alfvén speed [*Hasegawa*, 1976; *Goertz*, 1984]. Another possible mechanism involves coupling between the shear mode and the compressional wave, which propagates transverse to the ambient magnetic field [*Chen and Hasegawa*, 1974; *Southwood*, 1974; *Inhester*, 1987]. For either mechanism a large-amplitude response occurs on the L shell where the frequency of the large-scale "driver" matches one of the field line eigenfrequencies, determined by the length of the magnetic field line and the distribution of background Alfvén speed along it. Energy is transferred from the external driver to a shear Alfvén wave standing along geomagnetic field lines on this L shell. This process is called field line resonance (FLR). More than 2 decades of observations have confirmed the basic phenomenon (see *Samson et al.* [1992] for references), with more recent measurements providing a good correlation with the occurrence of small-scale auroral arcs [*Samson et al.*, 1991, 1996; *Xu et al.*, 1993].

As energy is transferred from the external driver to the field line resonant oscillation, the amplitude of the resonant oscillation increases while its effective transverse scale size decreases until dispersion becomes important. At this point the resonance begins to radiate dispersive Alfvén waves which propagate energy away from the resonance layer in the perpendicular directions. This mechanism can saturate the growth in amplitude of the resonant oscillation and limits the contraction of its transverse structure.

Owing to the intrinsic inhomogeneity of the magnetospheric plasma and geomagnetic field, two types of dispersion can affect small-scale Alfvén waves that propagate between the equatorial magnetosphere and ionosphere. In the relatively cold, low-altitude plasma, where the Alfvén speed is much larger than the electron thermal speed, the dispersion is due to the finite electron inertia (inertial dispersion) [*Goertz and Boswell*, 1979; *Lysak and Carlson*, 1981]. In the hot, equatorial magnetospheric plasma where the Alfvén speed is less than the electron thermal speed and where electron inertial effects can be neglected, the dispersion is due to the finite plasma temperature (kinetic dispersion) [*Hasegawa*, 1976].

An important difference between these two types of dispersion is the fact that the transverse group velocity of a kinetic Alfvén wave is opposite to that of an inertial Alfvén wave. As a consequence of this effect, a small-scale FLR radiates inertial Alfvén waves along the transverse gradient of v_A at low altitude [*Goertz and Boswell*, 1979], whereas it radiates kinetic Alfvén waves in the opposite direction in the equatorial magnetosphere [*Hasegawa*, 1976]. It was shown by *Streltsov and Lotko* [1995] (hereinafter referred to as SL95) that the opposing inertial and kinetic dispersions on different parts of the magnetic flux tube can cause small-scale, dispersive Alfvén waves to be trapped inside the resonance layer. When this occurs, the dispersive FLR is termed "nonradiative," and it can reach significantly larger amplitude and contract to much smaller transverse scale than radiative FLRs.

The fine structure of dispersive, nonradiative FLRs for the first three odd harmonics was investigated on the basis of a linear, reduced, two-fluid MHD model [*Chmyrev et al.*, 1988] in a "box" geometry (with constant ambient magnetic field and electron temperature) by *Streltsov and Lotko* [1996] (hereinafter referred to as SL96) and in a dipole magnetic field geometry with realistic magnetospheric parameters by *Streltsov and Lotko* [1997] (hereinafter referred to as SL97). These investigations show that FLRs can become nonradiative on auroral L shells. While these previous studies necessarily included the combined dispersive effects of finite electron inertia and finite plasma thermal energy, kinetic dispersion is provided entirely by the finite electron temperature via the parallel electron equation of motion. In fact, auroral field lines typically thread the magnetospheric region where the ion temperature exceeds the electron temperature, so one expects dispersive effects of the finite ion Larmor radius to influence the dynamics of a contracting FLR. In this paper, the two-fluid MHD model of SL97 is extended in dipole geometry to include finite ion Larmor radius effects. It is shown that such effects can have a profound influence on the ability of the dispersive Alfvén wave to develop a parallel electric field in the equatorial magnetosphere. As a consequence, it is shown that the parallel electric field of a dispersive FLR is confined largely to the lower magnetosphere where electron inertial dispersion is activated.

2. Model

As in the earlier work by SL97, this study will consider parameters appropriate to the formation of dispersive FLRs on geomagnetic field lines passing through the inner edge of the nightside plasma sheet (about $L = 7$–8). Interest in this particular region is motivated by the fact that (1) it maps along dipolar magnetic field lines to the ionosphere near 70^0 geomagnetic latitude, where large-amplitude, small-scale transverse electric fields are predominantly measured by low-altitude satellites [*Bennett et al.*, 1983; *Karlsson and Marklund*, 1996], and (2) a statistical survey of magnetospheric ULF waves by *Zhu and Kivelson* [1991] has shown that dominantly toroidal magnetic oscillations with characteristics indicative of fundamental or odd harmonic FLRs are most intense near the inner edge of the premidnight plasma sheet.

Plasma in this region is assumed to be magnetized, low β ($\beta \equiv 8\pi P/B_0^2 \ll 1$, here P is the plasma gas pressure), collisionless, and initially free from any bulk motion or electric currents. In such a plasma, magnetically incompressible (shear) Alfvén waves and com-

pressible fast mode waves essentially decouple from the slow mode [*Hasegawa and Uberoi*, 1982; *Kouznetsov and Lotko*, 1995]. Near the resonant surface the plasma response is primarily magnetically incompressible [*Hasegawa and Uberoi*, 1982], so coupling between the shear and compressible waves may be neglected in the vicinity of the resonant surface as well. This fact significantly simplifies the model, reducing it to only three scalar equations coupling the electric potential ϕ, the parallel component of the vector potential (flux function) $A_\parallel$, and the disturbed part of the quasi-neutral plasma density n_1.

The azimuthal variation of solutions is ignored as a first approximation because observations show that FLRs and associated auroral structures are narrow in latitude and practically homogeneous in local time [*Greenwald and Walker*, 1980; *Samson et al.*, 1991]. Two-dimensionality eliminates the strong convective and magnetic nonlinearities in the model, and only weak nonlinear terms associated with the density perturbation survive. The density nonlinearities are at least of the next order of smallness compared with other terms in the model equations and are therefore negligible for the amplitudes of solutions considered in this paper. Further details of the validity of the linear model are discussed by SL96. Some nonlinear effects that arise in the three-dimensional dynamics of large-scale FLR in the Earth's magnetosphere are treated by *Rankin et al.* [1993, 1995].

The linearized, two-dimensional model that is investigated in the paper includes the electron parallel momentum equation

$$m_e n_0 \frac{\partial v_{\parallel e}}{\partial t} + e n_0 E_\parallel + \hat{\mathbf{b}}\cdot\nabla p_e = 0 \qquad (1)$$

the density continuity equation

$$\frac{\partial n_1}{\partial t} + \nabla\cdot n_0 v_{\parallel e}\hat{\mathbf{b}} = 0 \qquad (2)$$

and the current continuity equation combined with the ion momentum equation

$$\left(1-\rho_i^2\nabla_\perp^2\right)\nabla\cdot j_\parallel\hat{\mathbf{b}} + \frac{c^2}{4\pi}\nabla\cdot\left(\frac{1}{v_A^2}+\frac{1}{c^2}\right)\frac{\partial}{\partial t}\mathbf{E}_\perp = 0 \qquad (3)$$

Here the subscripts $\parallel$ and $\perp$ denote vector components in the directions locally parallel and perpendicular to $\mathbf{B}_0$, respectively; v_e is the electron speed; n_0 is the background quasi-neutral plasma density; $\mathbf{E}_\perp = -\nabla_\perp\phi$; $E_\parallel = -\hat{\mathbf{b}}\cdot\nabla\phi - (1/c)\partial A_\parallel/\partial t$; $\hat{\mathbf{b}} = \mathbf{B}_0/B_0$; $p_e = n_1 T_e$; T_e and T_i are background electron and ion temperatures, respectively; $j_\parallel = -e n_0 v_{\parallel e} = -(c/4\pi)\nabla_\perp^2 A_\parallel$; $\rho_i = T_i^{1/2}/m_i^{1/2}\omega_{ci}$ is ion Larmour radius; and $v_A^2 = B_0^2/4\pi n_0 m_i$.

The current continuity equation (3) includes the displacement current, important when the Alfvén speed approaches the speed of light, and full ion Larmor radius correction. It is significantly different from the classical two-fluid MHD model [e.g., *Chmyrev et al.*, 1988], and its derivation requires some additional explanation.

2.1. Full Larmour Radius Correction

The current continuity equation, neglecting the displacement current, is:

$$\nabla\cdot\mathbf{j}_\parallel + \nabla\cdot\mathbf{j}_\perp = 0 \qquad (4)$$

In the model the parallel current, $\mathbf{j}_\parallel = j_\parallel\hat{\mathbf{b}}$, is carried by electrons only [*Chmyrev et al.*, 1988]. The perpendicular current, $\mathbf{j}_\perp = e n_0(\boldsymbol{v}_{\perp i} - \boldsymbol{v}_{\perp e})$, appears from a small difference in perpendicular velocities of ions and electrons. This difference, in turn, arises from (1) ion inertia and (2) the small-scale size of dispersive waves transverse to the geomagnetic field.

It was shown by *Kadomtsev* [1965] that when the transverse scale size of the electromagnetic wave becomes comparable with the ion Larmour radius, the electric drift of the ion guiding center is determined by the effective electric field which is smaller than electric field in the center of the Larmor circle by a factor of $I_0(s)e^{-s}$, where $s = \rho_i^2 k_\perp^2$ and I_0 is a modified Bessel function. This effect combined with the effect of finite ion mass leads to the next expression for the Fourier transform [$\tilde{\mathcal{F}}(k_\perp) = \int \mathcal{F}(r)e^{-i\mathbf{k}_\perp\cdot\mathbf{r}}dr$] of the perpendicular current [*Cheng*, 1991]:

$$\tilde{\mathbf{j}}_\perp = \frac{c^2}{4\pi}\frac{1}{v_A^2}\frac{1-I_0(s)e^{-s}}{s}\frac{\partial}{\partial t}\tilde{\mathbf{E}}_\perp \qquad (5)$$

This form of the perpendicular current is obtained under the assumption that the scale size of the solution ($\sim 1/k_\perp$) is much smaller than the scale size of inhomogeneities in the background v_A and ρ_i transverse to the ambient magnetic field.

To express the perpendicular current in the spatial domain, some approximation of the term $[1 - I_0(s)e^{-s}]/s$ must be made before the inverse Fourier transform from (5) can be taken. Depending on the magnitude of s, three different situations are possible.

First, if $s = 0$, then $[1 - I_0(s)e^{-s}]/s = 1$, and (4) becomes

$$\nabla\cdot j_\parallel\hat{\mathbf{b}} + \frac{c^2}{4\pi}\nabla\cdot\frac{1}{v_A^2}\frac{\partial}{\partial t}\mathbf{E}_\perp = 0 \qquad (6)$$

Equations (1), (2), and (6) form a classical reduced two-fluid MHD model (sometimes called Strauss equations). It has been intensively investigated in the context of dispersive Alfvén waves and instabilities in tokamak plasma by *Strauss* [1976], *Morrison and Green* [1980], *Morrison and Hazeltine* [1984], *Hazeltine and Meiss* [1985], as well as in the magnetospheric plasma by *Lysak and Dum* [1983], *Seyler* [1988, 1990], *Chmyrev et al.* [1988, 1992], SL95, and SL97.

Second, if $s \ll 1$, then $[1 - I_0(s)e^{-s}]/s \approx 1 - (3/4)s$ [*Hasegawa*, 1976]. It leads to an alternative expression for (4):

$$\nabla\cdot j_\parallel\hat{\mathbf{b}} + \frac{c^2}{4\pi}\nabla\cdot\frac{1}{v_A^2}\left(1+\frac{3}{4}\rho_i^2\nabla_\perp^2\right)\frac{\partial}{\partial t}\mathbf{E}_\perp = 0 \qquad (7)$$

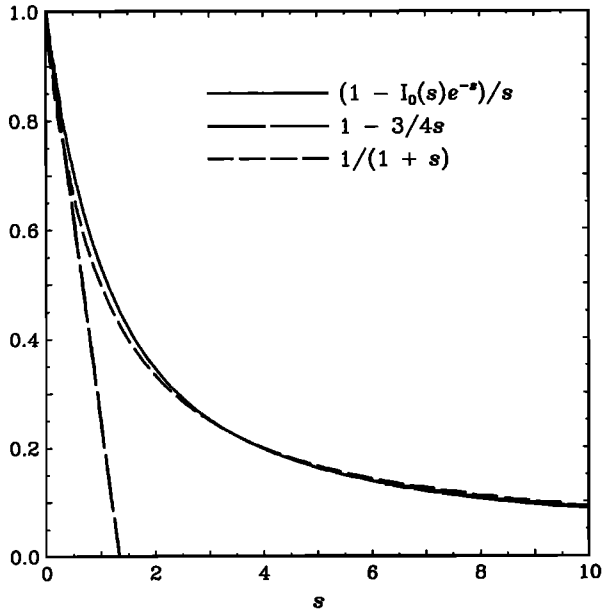

Figure 1. Approximations of the ion kinetic term in the expression for the perpendicular current (5).

Third, if s is of the order of or larger than unity, then $[1 - I_0(s)e^{-s}]/s \approx 1/(1+s)$. This is the so-called Padé approximation [*Johnson and Cheng*, 1997]. In this case, (4) will take the form

$$(1 - \rho_i^2 \nabla_\perp^2)\, \nabla \cdot j_\parallel \hat{\mathbf{b}} + \frac{c^2}{4\pi} \nabla \cdot \frac{1}{v_A^2} \frac{\partial}{\partial t} \mathbf{E}_\perp = 0 \qquad (8)$$

Figure 1 demonstrates that the Padé approximation of the term $[1 - I_0(s)e^{-s}]/s$ is suitable for the entire range of s; it is almost as accurate as the approximation used by *Hasegawa* [1976] when $s \leq 0.25$ (both approximations give a relative error here of less than 5%), and it is still reasonable for larger values of s (the relative error there is about 6%), where the other approximation cannot be applied at all. The model, including finite Larmour radius correction in the same form as (8), was developed from different assumptions by *Hazeltine et al.* [1987].

Finally, to get (3) from (8) the divergence of the displacement current should be included for cases when v_A is not negligible compared with the speed of light. Such a situation can occur on auroral field lines in the lower magnetosphere (see Figure 2) when the plasma density becomes very small for example, in an auroral plasma cavity [*Persoon et al.*, 1988].

2.2. Dispersion Relations

Parameters of the background plasma and magnetic field can change by a factor of 100–1000 along an auroral field line from the ionosphere to the equatorial magnetosphere. This strong inhomogeneity complicates the derivation and analysis of the dispersion relation for long, parallel wavelength Alfvén waves propagating or standing on auroral field lines [*Lysak and Lotko*, 1996]. The dispersion relations given below are used only for qualitative explanation of the behavior of small-scale dispersive waves observed in the subsequent numerical experiments. To this end, the resonant magnetic flux tube is divided into three parts depending on the ratio between $\lambda^2 = c^2/\omega_{pe}^2$ and $\rho^2 = \rho_i^2(1+T_e/T_i) = \rho_i^2+\rho_s^2$ (Figure 2); for purposes of the dispersion analysis only, the plasma is taken to be weakly (parametrically) inhomogeneous in each region.

At low altitudes (region I in Figure 2) the plasma is relatively cold, $\lambda^2 \gg \rho^2$, and v_A here is not necessarily small compared with the speed of light. The dispersion relation deduced from the model in this region is

$$\omega^2 = k_\parallel^2 \frac{v_A^2}{1 + v_A^2/c^2} \left(1 + k_\perp^2 \lambda^2\right)^{-1} \qquad (9)$$

The parallel electric field here is proportional to $k_\perp^2 \lambda^2$, and it can be written in terms of the scalar potential ϕ as

$$E_\parallel = -ik_\parallel \frac{k_\perp^2 \lambda^2}{1 + k_\perp^2 \lambda^2} \phi \qquad (10)$$

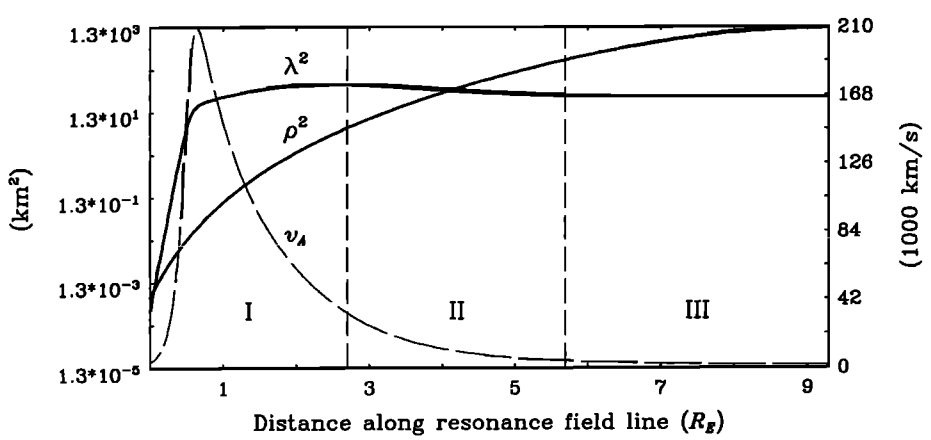

Figure 2. Profiles of the background $\rho^2 = \rho_i^2(1 + T_e/T_i)$, $\lambda^2 = c^2/\omega_{ci}^2$ (solid curves), and $v_A = B_0/\sqrt{4\pi n_0 m_i}$ (long-dashed curve) along the resonance field line from the ionosphere to the equatorial plane. Here $\rho_i = T_i^{1/2}/m_i^{1/2}\omega_{ci}$ is ion Larmour radius; T_e and T_i are electron and ion temperatures, respectively; and ω_{ci} is ion cyclotron frequency.

Because $\lambda^2 \sim 1/n_0$, from (10) one may expect the strongest parallel electric fields and hence particle acceleration to occur at low altitudes when the plasma is very tenuous, e.g., in an auroral plasma cavity [*Persoon et al.*, 1988].

In the near-equatorial magnetosphere (region III in Figure 2) the electron thermal speed is larger than Alfvén speed and $\lambda^2 \ll \rho^2$. The dispersion relation of the model here is

$$\omega^2 = k_\parallel^2 v_A^2 \left(1 + k_\perp^2 \rho^2\right) \tag{11}$$

Here the parallel electric field expressed via the scalar potential ϕ is

$$E_\parallel = ik_\parallel \frac{k_\perp^2 \rho_s^2}{1 + k_\perp^2 \rho_i^2} \phi \tag{12}$$

Expression (12) shows that in the hot magnetospheric plasma the parallel electric field of the dispersive Alfvén waves increases with increasing electron temperature and decreases with the increasing ion temperature. This means that in the equatorial magnetosphere the parallel electric field of dispersive Alfvén waves should be very small because magnetospheric ions in the near-Earth plasma sheet are typically hotter than electrons. This result is also in good agreement with the finding by *Lysak and Lotko* [1996] that hot ions reduce Landau damping of small-scale dispersive Alfvén waves, which is connected with the parallel electric field of these waves.

In the intermediate region II in Figure 2, where $\lambda^2 \approx \rho^2$ and $v_A \ll c$, the dispersion relation of the model is

$$\omega^2 = k_\parallel^2 v_A^2 \left(1 + k_\perp^2 \rho^2\right) \left(1 + k_\perp^2 \lambda^2\right)^{-1} \tag{13}$$

The parallel electric field in this region is

$$E_\parallel = ik_\parallel \left(1 + k_\perp^2 \rho_i^2\right)^{-1} \left(k_\perp^2 \rho_s^2 - \frac{\omega^2}{k_\parallel^2} \frac{1}{v_A^2} k_\perp^2 \lambda^2\right) \phi \tag{14}$$

There are at least two points of interest in the behavior of the dispersive Alfvén wave in this particular region. The first one is the reversal of sign of the perpendicular component of the wave group speed $v_{g\perp}$ at the transition point where $\lambda^2 = \rho^2$. Indeed, from (13) it is easy to see that

$$v_{g\perp} = \frac{dw}{dk_\perp} = k_\perp k_\parallel v_A \frac{\rho^2 - \lambda^2}{(1 + k_\perp^2 \rho^2)^{1/2} (1 + k_\perp^2 \lambda^2)^{3/2}} \tag{15}$$

Thus an oblique wave propagating toward higher L shells near the equator, for example, will begin moving toward lower L shells after passing through the transition region. This effect makes possible the confinement of dispersive Alfvén waves in the resonance layer and enables the formation of nonradiative FLR layers (SL95).

The second point is that in the transition region the phase speed is close to that predicted by classical dispersion relation for one-fluid, shear Alfvén waves $\omega^2 = k_\parallel^2 v_A^2$; however, this wave has a parallel electric field:

$$E_\parallel = -ik_\parallel \frac{k_\perp^2 \rho_i^2}{1 + k_\perp^2 \rho_i^2} \phi \tag{16}$$

This field originates from the kinetic treatment of hot ions and does not appear in one- or two-fluid MHD descriptions of small-scale Alfvén waves. Actually, (13) and (14) state that in the homogeneous magnetized plasma with background parameters such that $\lambda^2 = \rho^2$, small-scale Alfvén waves with any finite $k_\perp$ will propagate exactly along the ambient magnetic field lines, satisfy the classical dispersion relation for shear Alfvén waves, and carry parallel electric field defined by (16).

Hot ions also modify $E_\parallel$ in the region where $v_A = v_{Te}$ (without ion correction, $E_\parallel = 0$ at this point) and where the electron Landau damping of the wave, which is the main mechanism of the wave energy dissipation in the collisionless plasma near this point, might occur. Unfortunately, owing to the complexity of the problem, Landau damping has not been investigated for the situation when the parallel wavelength is much larger than the parallel scale size of plasma inhomogeneity or of the transition region (the situation of particular interest here). Nevertheless, because the wave spends only a small fraction of its period in the transition/dissipation region [*Lysak and Lotko*, 1996], Landau damping of the dispersive Alfvén waves is not expected to dominate the global wave dynamics, so that the main features of numerical results given in section 4 are preserved.

2.3. Background Parameters

The part of the nightside magnetosphere modeled in the paper is confined by $L = 7.25$ and $L = 7.75$ magnetic shells. The conducting ionosphere at 320 km altitude, near the F layer density maximum, forms the top and bottom boundaries of the domain. In this region, (1)–(3) are investigated in orthogonal dipolar coordinates (L, φ, μ), defined in terms of spherical polar coordinates (r, φ, θ) as [*Radoski*, 1967; *Cummings et al.*, 1969]

$$L = \frac{r}{R_E \sin^2\theta}, \quad \varphi, \quad \mu = \frac{\cos\theta}{r^2},$$

with corresponding metric factors:

$$h_L = \frac{R_E \sin^3\theta}{(1 + 3\cos^2\theta)^{1/2}}, \quad h_\varphi = r\sin\theta,$$

$$h_\mu = \frac{r^3}{(1 + 3\cos^2\theta)^{1/2}}.$$

Here $R_E = 6400$ km is the Earth radius. The unit vector $\hat{\mathbf{L}}$ is locally perpendicular to the magnetic shell, directed outward from the Earth; $\hat{\boldsymbol{\varphi}}$ is directed locally eastward perpendicular to meridional planes; and $\hat{\boldsymbol{\mu}}$ is directed locally along $\mathbf{B}_0$ (see SL97, Figure 1).

The dipole background geomagnetic field varies as

$$B_0 = 31{,}000 \frac{R_E^3}{r^3} \left(1 + 3\sin^2\theta\right)^{1/2} \text{nT} \tag{17}$$

The background plasma density $n_0(L, \mu)$ is modeled as

$$n_0(L, \mu) = n_{00}(\mu) \left[1 + n_{01}(L) n_{02}(\mu)\right] \tag{18}$$

Here $n_{00}(\mu)$ determines the density profile along the resonant field line ($L = 7.5$):

$$n_{00}(\mu) = 99995.5\, e^{-20(r-1.05)} + 4.08\, r^{-3} + 0.99 - 0.67\left[e^{-\left(\frac{r-3}{2.5}\right)^2} - e^{-\left(\frac{7.5-3}{2.5}\right)^2}\right] \text{ cm}^{-3} \quad (19)$$

Expression (19) provides plasma density of 10^5 cm^{-3} at the altitude 320 km, 0.96 cm^{-3} at geocentric distance 2 R_E, 0.5 cm^{-3} at geocentric distance 3 R_E, and 1 cm^{-3} in the equatorial magnetosphere at geocentric distance 7.5 R_E. The density model therefore includes a plasma density depletion, which is often observed at radial distance 2–5 R_E in the nightside auroral zone [*Persoon et al.*, 1988].

The function $n_{01}(L) = \tanh[(L - 7.5)/0.04375]$ determines the plasma inhomogeneity in the direction transverse to the resonant field line, and $n_{02}(\mu) = 0.5/\exp(4\ell/\mathcal{L})^2$ (here $\ell = \ell(\mu)$ is the distance along the resonant field line measured from the equator and $\mathcal{L} \approx 18.6$ is the total length of the resonant field line) determines the distribution of the transverse plasma inhomogeneity along the resonant field line. This choice of $n_{02}(\mu)$, in effect, confines the transverse gradient in density to the near-equatorial magnetosphere where a field line resonance will be stimulated.

Observations of the localized density gradients like one modeled here, in the outer ring current/near-Earth plasma sheet region, are reported in the literature [*Hughes and Grard*, 1984; SL95]. These observations are discussed in more detail in SL95. The dependence of the spatiotemporal properties of the FLR solutions on the parameters of the density gradient and on its location was investigated by SL97.

The background electron temperature is modeled in the paper as

$$T_e(L,\mu) = \frac{T_{e*}}{(4.08\, r^{-3} + 0.99)[1 + n_{01}(L) n_{02}(\mu)]}$$

here r is the same geocentric distance as used in (19). The background ion temperature is modeled as $T_i(L,\mu) = (T_{i*}/T_{e*})T_e(L,\mu)$. Here $T_{e*} = 150$ eV and $T_{i*} = 500$ eV are constants estimated in the nightside equatorial magnetosphere near $L = 7.5$ using an empirical model by *Moore et al.* [1987] and Active Magnetospheric Particle Tracer Explorers/Ion Release Module (AMPTE/IRM) data. That choice of the function for T_e and T_i provides the equilibrium requirement that $\mathbf{B}_0 \cdot \nabla(n_0 T_e) = 0$ in the hot, higher-altitude, magnetospheric plasma. It also provides a gradual reduction of the plasma temperature in going from the equator line to the ionosphere along the flux tube. For these parameters of the background plasma and magnetic field in the nightside equatorial magnetosphere near $L = 7.5$, the plasma β there is equal to 0.05, so the low-β assumption of the model is satisfied. Of course, the plasma β can be larger in this region if a small population of energetic particles with low density will be taken into account. Although these particles make the plasma β larger, they basically do not affect the Alfvén waves which are carried by the cold, dense core plasma. Because the higher-energy particles have small density, they have a small effect on the analysis, and the relevant β for the problem is that of the core plasma given above. This specification of functions for B_0, n_0, T_i, T_e, and their magnitudes in the equatorial magnetosphere provides distributions of v_A, λ^2, and ρ^2 along the resonant field line as shown in Figure 2.

3. Numerical Computations

To investigate numerically spatiotemporal behavior of the small-scale, dispersive FLR on auroral magnetic field lines, it is convenient to rewrite (1)–(3) in the dimensionless form:

$$\frac{\partial}{\partial t}\left(n_0 A_\parallel - \delta \nabla_L^2 A_\parallel\right) = -n_0 \nabla_\mu \phi + \nabla_\mu (T_e n_1) \quad (20)$$

$$\frac{\partial n_1}{\partial t} = -B_0 \nabla_\mu \left(\frac{1}{B_0} \nabla_L^2 A_\parallel\right) \quad (21)$$

$$\frac{\partial}{\partial t} \nabla \cdot \left(\frac{1}{v_A^2} + \frac{1}{c^2}\right) \nabla_L \phi = -\left(1 - \rho_i^2 \nabla_L^2\right) B_0 \nabla_\mu \left(\frac{1}{B_0} \nabla_L^2 A_\parallel\right) \quad (22)$$

where

$$\delta = \frac{m_e}{m_i} \frac{B_{0*}^2}{4\pi n_* T_{e*}}; \quad \nabla_\mu = \frac{1}{h_\mu}\frac{\partial}{\partial \mu}; \quad \nabla_L = \frac{1}{h_L}\frac{\partial}{\partial L};$$

$$\nabla_L^2 A_\parallel = \frac{1}{h_L h_\varphi} \frac{\partial}{\partial L}\left(\frac{h_\varphi}{h_L h_\mu} \frac{\partial h_\mu A_\parallel}{\partial L}\right);$$

$$\nabla \cdot \left(\frac{1}{v_A^2} + \frac{1}{c^2}\right) \nabla_L \phi = \frac{1}{h_L h_\varphi h_\mu} \frac{\partial}{\partial L}\left(\frac{1}{v_A^2} + \frac{1}{c^2}\right) \frac{h_\varphi h_\mu}{h_L} \frac{\partial \phi}{\partial L}.$$

Dimensionless variables include [*Chmyrev et al.*, 1988]

$$t = t/\omega_{ci^*}; \quad l_\perp = \frac{c_{s^*}}{\omega_{ci^*}} l_\perp; \quad l_\parallel = \frac{v_{A^*}}{\omega_{ci^*}} l_\parallel; \quad T_e = T_{e*} T_e;$$

$$\phi = \frac{T_{e*}}{e}\phi; \quad A_\parallel = \frac{T_{e*} c}{e v_{A^*}} A_\parallel; \quad n = n_* n.$$

Here T_{e*}, ω_{ci^*}, c_{s^*}, v_{A^*}, and n_* are constants estimated in the nightside equatorial magnetosphere at radial distance 7.5 R_E.

The main computational difference between this model and the two-fluid MHD model considered by SL97 is the fact that now, owing to the ion kinetic modification of the current continuity equation, n_1 cannot be expressed as $\nabla \cdot (1/v_A^2 + 1/c^2) \nabla_L \phi$. As a result, the model cannot be reduced further to only two equations and the entire set of (20)–(22) must be solved.

Otherwise, the numerical algorithm applied here is the same as that described in SL97. A fourth-order "predictor-corrector" method is used to time advance the numerical solution. The Adams-Bashforth (AB)

four-step method is used as a "predictor" and the Adams-Moulton (AM) three-step method is used as a "corrector" [*Burden and Faires*, 1989]. In this approach, new values of ϕ and n_1 at each time step are obtained on the inner grid nodes from the predictor (AB) part of the algorithm. Then these new values are used to calculate $A_\parallel$ from the corrector (AM) part. This "splitting" of the computation in time improves accuracy and significantly reduces the amount of numerical operations compared with a total predictor-corrector scheme for the entire system (20)–(22).

Owing to the simple rectangular geometry of the computational domain in the orthogonal dipolar coordinate (L, μ), spatial differential operators in (20)–(22) are approximated using a finite difference approach. To get better resolution without additional computational expense, ϕ, n_1, and $A_\parallel$ are approximated on grids shifted along field lines. The computational grid for ϕ and n_1 contains 101 levels along field lines, including both ionospheric boundaries. The grid for $A_\parallel$ contains 100 levels along field lines and starts a half step above the ionospheric boundary. In the L direction both grids have 151 equally spaced levels, including both lateral boundaries. Details of the numerical algorithm, particularly the techniques for calculating $A_\parallel$ and ϕ at each time step from the corresponding elliptic equations, are given in the appendix.

Without significant loss of generality, the ionospheres in the calculations described below are treated as perfectly conducting plates, where the tangential electric field vanishes and the electric potential function ϕ is set equal to zero. This ideal ionospheric boundary condition is a reasonable approximation because the Pedersen conductivity of the auroral ionosphere is typically much larger than the Alfvén conductivity [*Vickrey et al.*, 1981; *Spiro et al.*, 1982]; consequently, Alfvén waves are almost perfectly reflected by the ionosphere [*Mallinckrodt and Carlson*, 1978].

In the two-dimensional simulations described below, a FLR on $L = 7.5$ magnetic shell is excited by a generator localized on the right/tailward lateral boundary ($L = 7.75$) of the computational domain within a region $\pm\mathcal{L}/12$ about the equator. A generator of this type can be considered as a model of electromagnetic disturbances confined to the nightside plasma sheet, for example, disturbances that might arise during the growth phase of a substorm. To excite the fundamental or any odd-harmonic FLRs, the perpendicular electric field of the generator should be symmetrical to the equator, so the boundary condition for ϕ is set as

$$\phi(\mu, t) = \phi_0 \sin(\omega t)\, e^{-(12\ell/\mathcal{L})^2} \tag{23}$$

The boundary condition for the flux function $A_\parallel$ on the right boundary is calculated from (20) as a surface wave solution (second-order derivatives in L far from the resonant shell are negligible), $\partial_t A_\parallel = -\nabla_\mu \phi$:

$$A_\parallel(\mu, t) = -\frac{\phi_0}{\omega} \cos(\omega t)\, e^{-(12\ell/\mathcal{L})^2} \frac{288\ell}{\mathcal{L}^2} \nabla_\mu \ell$$

Both ϕ and $A_\parallel$ are kept equal to 0 on the left/earthward lateral boundary. Because energy is pumped into the resonance layer via the long-range field of the surface wave [*Hasegawa*, 1976; SL1], it is unimportant, from a numerical point of view, which lateral boundary, left or right, is driven.

Because the geomagnetic oscillations with very discrete, monochromatic frequencies are permanently observed in the auroral region on the ground [*Samson et al.*, 1992; *Rankin et al.*, 1993], as well as on the satellites [*Hughes and Grard*, 1984], the investigation presented in this paper are restricted by the case of the monochromatic driver only. So the frequency ω of the generator (23) is taken to be the eigenfrequency of the solution to the classical, one-fluid MHD eigenvalue problem for a toroidal ULF wave standing on the $L = 7.5$ dipole magnetic shell [*Radoski*, 1967; *Cummings et al.*, 1969; *Cheng et al.*, 1993]. In particular, to find the eigenfrequencies of FLR, the next second-order, ordinary differential equation for the function $\mathcal{F} = h_\mu E_L / h_\varphi$, modified from *Cummings et al.* [1969] by including relativistic correction (displacement current), is solved with an appropriate boundary condition ($E_L = 0$) on the ionospheres:

$$\frac{1}{h_\varphi^2} \frac{1}{B_0} \frac{1}{h_\mu} \frac{\partial}{\partial \mu} \left(h_\varphi^2 B_0 \frac{1}{h_\mu} \frac{\partial \mathcal{F}}{\partial \mu} \right) + \omega^2 \left(\frac{1}{v_A^2} + \frac{1}{c^2} \right) \mathcal{F} = 0 \tag{24}$$

For the parameters of the background plasma and magnetic field given above, the eigenfrequencies of the first three odd harmonics obtained from (24) on $L = 7.5$ are found to be 11.4 mHz for the fundamental mode, 49.8 mHz for the third harmonic, and 88.2 mHz for the fifth harmonic.

These harmonic eigenfrequencies are higher than FLR frequencies at 1.3, 1.9, or 2.6 mHz reported from the ground-based observations [*Samson et al.*, 1992]; but because dispersive, harmonic FLRs usually produce very narrow, multiple electromagnetic structures, there is almost no chance that their magnetic field/frequency can be measured on the ground owing to the strong attenuation of small-scale signals by the atmosphere-ionosphere system [*Hughes and Southwood*, 1976]. At the same time, because geomagnetic FLRs with frequencies up to 80 mHz are statistically measured on satellites at high latitudes [*Andersen et al.*, 1990; *Hughes and Grard*, 1984], we find it reasonable to mention these frequencies here for completeness.

4. Results and Discussion

Numerical investigation of the model described by (1)–(3) shows that for the background plasma and magnetic field parameters given in section 2.3, FLR for the fundamental mode becomes nonradiative on $L = 7.5$. In our terminology, nonradiative FLR means that the temporal variation of the FLR amplitude is localized transverse to the geomagnetic field to the vicinity of the resonance location. As an example, the profile of E_L across the magnetic field lines in the equatorial plane

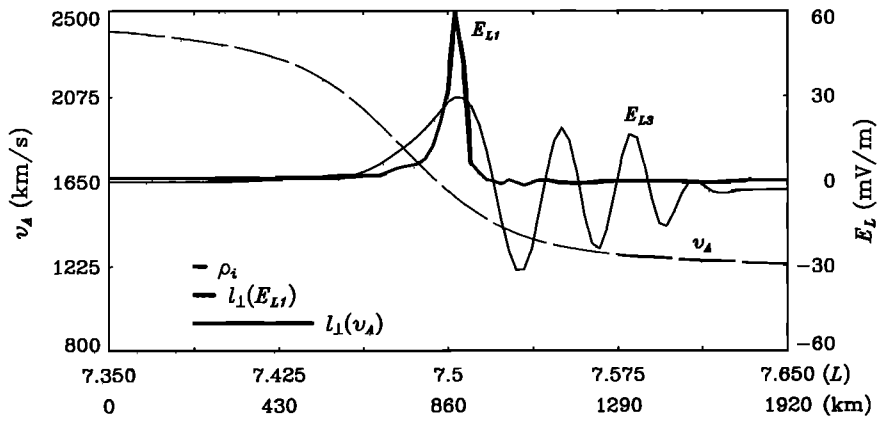

Figure 3. Profiles of the perpendicular electric field E_L of the fundamental field line resonance (FLR) at time 2557 s (thick solid curve marked E_{L1}), E_L of the third-harmonic FLR at time 293 s (thin solid curve marked E_{L3}), and background v_A (dashed curve), plotted across the geomagnetic field in the equatorial magnetosphere.

for the nonradiative fundamental FLR at time 2557 s is shown in Figure 3 by the thick solid curve labeled E_{L1}. For comparison, the profile of E_L of the third-harmonic FLR, which is radiative under the same background conditions, is plotted in Figure 3 at time 293 s by the thin curve labeled E_{L3}. The main conclusion that follows from the comparison of these two curves is that the nonradiative FLR produces much more narrow, localized, and intense electromagnetic structures than FLRs radiating dispersive Alfvén waves.

Results from the computer simulations are first discussed by verifying the assumptions on which the model is based. Three characteristic transverse scale sizes are also shown in Figure 3: the ion Larmour radius (ρ_i = 31 km), the scale size of the resonant field defined as the full width of the peak in E_L at half amplitude [$l_\perp(E_L)$ = 55 km], and the scale size of the transverse inhomogeneity in the background Alfvén speed [$l_\perp(v_A)$ = 333 km]. First, Figure 3 shows that $l_\perp(v_A) \gg l_\perp(E_L)$, so the assumption in section 2.1 allowing application of a Fourier transform to $E_\perp$ in (5) is valid. Second, if the perpendicular wavelength of the resonant solution, defined as $l_{\perp r} \approx 2\, l_\perp(E_L) = 110$ km, implies $(k_\perp \rho_i)^2 = (2\pi\rho_i/l_{\perp r})^2 \approx 3.1$. This fact means that (1) hot magnetospheric ions should significantly modify the dispersive properties of the small-scale Alfvén waves and (2) dispersive Alfvén waves with such a small transverse wavelength are not accurately described using the small ion Larmor radius approximation [*Hasegawa*, 1976].

Figure 4 shows profiles of E_L, B_φ, E_μ, j_μ (solid curves), and ϕ_μ (dashed curve) along the resonant field line for the nonradiative, fundamental FLR, obtained as a numerical solution of (20)–(22) at time 2621 s. Magnitudes of the fields on these graphs, such as 182 mV/m for E_L and 0.11 mV/m for E_μ, were obtained by assuming that the maximum amplitude of E_L of the saturated FLR is equal to 200 mV/m (a typical value of the large-amplitude electric fields observed above the auroral ionosphere from a few thousand kilometers altitude up to about 2–2.5 R_E altitude [*Mozer*, 1981; *Weimer and Gurnett*, 1993]). With this choice the amplitude of any calculated quantity at any point in time and space is determined in a unique way owing to the linearity of the model.

Because the linear two-dimensional model considered here does not contain any volume or ionospheric boundary dissipation, the saturation of the resonance is due to (1) numerical dissipation, connected with using finite differences for the approximation of spatial derivatives, and (2) imperfect implementation of the nonradiative condition. As in SL97, numerical dissipation is the dominant saturation mechanism in these computations. In this sense the absolute saturation level of the FLRs computed in our model must be interpreted with caution. However, because numerical dissipation is determined by the parameters of the code (mostly by the spatial resolution), which are the same for all computations presented herein, it affects the behavior of all the FLR solutions in the same way and makes it meaningful to compare spatiotemporal properties of these FLRs with each other.

Figure 4 shows that, in many respects, the behavior of the nonradiative FLR calculated in the new model is qualitatively similar to that obtained by SL97 in a model without ion Larmour radius correction (Figure 4 in SL97). In particular, the perpendicular component of the electric field is enhanced at low altitudes at a distance of about 2 R_E along the resonant field line above the ionosphere: the amplitude of the transverse magnetic field and the field-aligned current density maximize at the ionospheric boundaries; the parallel potential drop between the ionosphere and $\approx$ 3 R_E altitude is sufficient to accelerate electrons into the ionosphere up to keV energies.

The main difference between results presented by SL97 and the results obtained from the model with full ion Larmour radius correction lies in the behavior of the parallel electric field at high altitudes. To illustrate this difference more explicitly, an additional computational

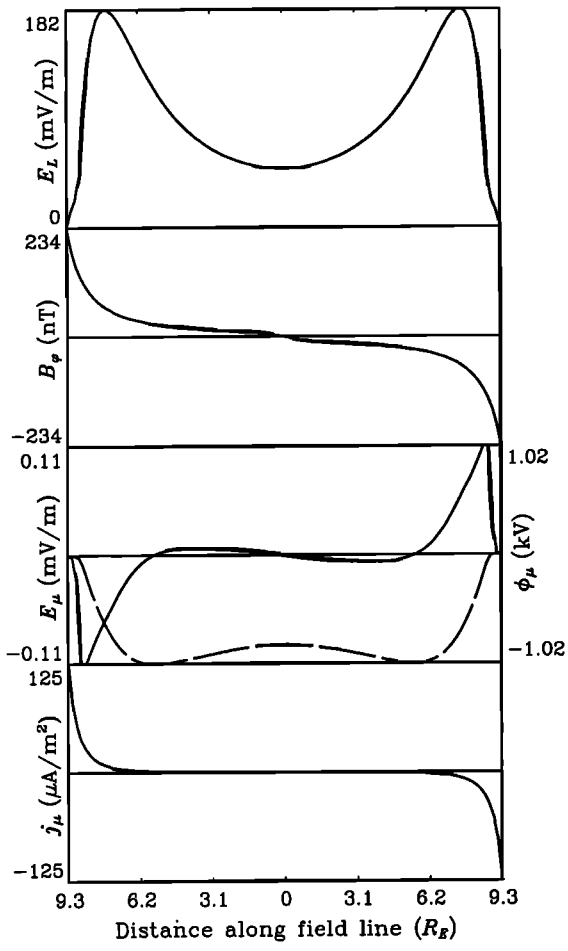

Figure 4. Profiles of the perpendicular electric field E_L, perpendicular magnetic field B_φ, parallel electric field E_μ, parallel current density j_μ (solid curves), and parallel potential ϕ_μ (dashed curve) along the resonant magnetic field line of the fundamental, nonradiative FLRs at time 2621 s.

run was performed. In this run, T_{i*} was set equal to 0, so the influence of hot ions was effectively "turned off." To maintain the same nonradiative balance between kinetic and inertial dispersions on the same magnetic L shell as before, T_{e*} was set equal to 650 eV. In that case the distribution of total $\rho^2 = \rho_i^2 + \rho_s^2$ along the resonance field line is the same as when $T_{i*} = 500$ eV and $T_{e*} = 150$ eV. The comparison between these two cases is shown in Figure 5.

Figures 5a and 5b show the evolution of the maximum of the amplitudes of E_L and E_μ in the computational domain for FLR with $T_{i*} = 500$ eV and $T_{e*} = 150$ eV (solid curves) and FLR with $T_{i*} = 0$ eV and $T_{e*} = 650$ eV (dashed curves). Graphs of E_L (Figure 5a) and E_μ (Figure 5b) show that both FLRs saturate on the same timescale and at the same amplitude level. This result is expected because the maximum of E_L and E_μ occur at low altitudes and is determined not by the plasma temperature but by the plasma density, which in both cases is the same. Figures 5c and 5d show the distribution of E_μ and ϕ_μ along the resonance field line at time 1955 s for the FLR with hot magnetospheric ions (solid curve) and for the FLR without ions (dashed curve). In agreement with (12) the parallel electric field in the high-altitude, near-equatorial plasma is almost eliminated when the kinetic dispersion is mostly provided by hot magnetospheric ions (solid curve in Figure 5c). As a result, the parallel potential distribution is nearly constant in this region (solid curve in Figure 5d). The amplitude of the parallel potential drop is also changed significantly. Despite the fact that the maximum amplitude of E_μ in both cases is almost the same (about 0.1 mV/m), the maximum of the parallel potential in the second case decreases by more than 25% compared with the case with hot ions included in the model.

As discussed in section 2.2, this effect means that even dispersive Alfvén resonances with extremely small transverse scale sizes will undergo only weak Landau damping in the magnetospheric plasma because the associated parallel electric field is significantly attenuated there by the hot ions.

The fact that higher-harmonic FLRs are much more "kinetically" radiative than the fundamental FLR for the same set of the background parameters is illustrated in Figure 3. Our investigation shows that even when the equatorial ions were "cooled" to 50 eV temperature, the third-harmonic FLR, on the $L = 7.5$ magnetic shell, continued to radiate kinetic dispersive waves. The same behavior of the harmonic FLRs in comparison with fundamental FLR was reported by SL97 in the model without hot magnetospheric ions, and it deserves additional investigation.

To understand the phenomenon, consider the ratio between perpendicular and parallel component of the group velocity of the dispersive Alfvén waves, $\boldsymbol{v}_g = d\omega/d\boldsymbol{k}$, at high and low altitudes. Because this analysis is mostly qualitative, it is sufficient to make use of the simplified dispersion relations derived in section 2.2. By using (9) and (11), it is easy to show that at the equatorial magnetosphere

$$v_{g\perp}/v_{g\|} = k_\| \frac{k_\perp \rho^2}{1 + k_\perp^2 \rho^2}, \tag{25}$$

and at low altitudes

$$v_{g\perp}/v_{g\|} = -k_\| \frac{k_\perp \lambda^2}{1 + k_\perp^2 \lambda^2} \tag{26}$$

So if different harmonic FLRs occur on the same magnetic L shell with the same parameters of the background plasma and contract to the same transverse scale size (or $k_\perp$), then the ratio $v_{g\perp}/v_{g\|}$ for the different harmonics differs in $k_\|$ only. At the equatorial magnetosphere, v_A is relatively homogeneous along the field line (Figure 2), so here it is reasonable to estimate $k_\| \sim \omega/v_A$. Because the eigenfrequency ω of higher harmonics is larger than that for the fundamental dispersive Alfvén wave, (25) shows that for the same value of $k_\perp^2 \rho^2$, the fundamental dispersive Alfvén wave propagates energy in the transverse direction more slowly than the harmonic waves for the same section of the resonance along the field line in the equatorial magnetosphere.

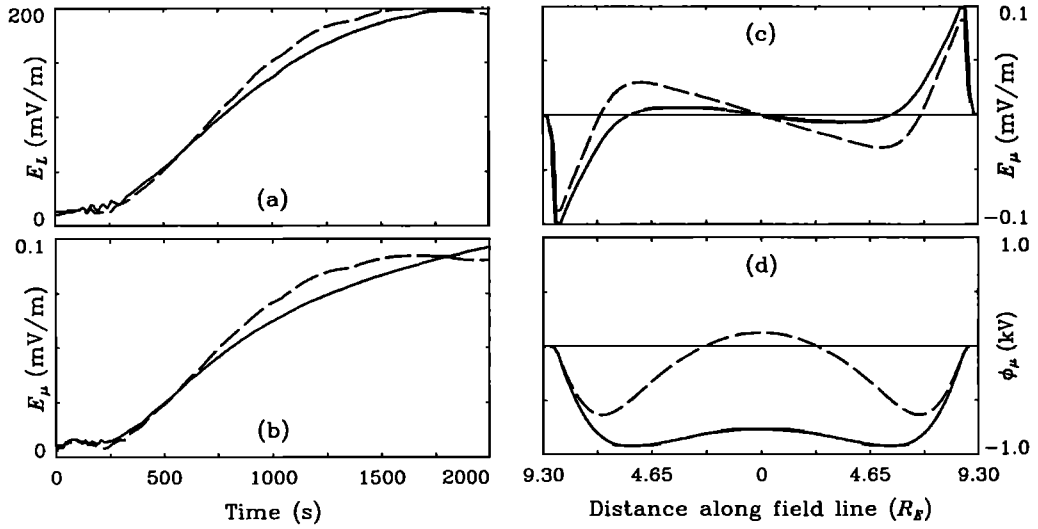

Figure 5. (a) Evolutions of maximum amplitudes of E_L of the fundamental nonradiative FLRs with ion temperature in the equatorial magnetosphere $T_{i*} = 500$ eV and electron temperature $T_{e*} = 150$ eV (solid curve) and $T_{i*} = 0$ eV and $T_{e*} = 650$ eV (dashed curve). (b) Evolution of maximum amplitudes of corresponding E_μ. (c) Profiles of E_μ from these two cases along the resonant magnetic field line at time 1955 s. (d) Profiles of the corresponding ϕ_μ.

At low altitudes, where the background Alfvén speed is very inhomogeneous, $k_\parallel$ cannot be replaced with ω/v_A, even as a rough approximation. Instead, the parallel structure of the fields obtained by solving the eigenvalue equation (24) can be analyzed. These fields can be considered as solutions of the entire model (1)–(3) during the "predispersive," one-fluid stage, wherein dispersive effects are not yet important. Figure 6 shows profiles of $E_\perp$ for the first four odd harmonics, calculated along the $L = 7.5$ magnetic shell using (24) and models for the background parameters given above. Because the immediate objective is to compare only the structure and not the amplitude of the solutions, each curve in Figure 6 is normalized to its own maximum value, so actually, $E_L/E_{L\max}$ for each harmonic is plotted. Figure 6 shows that at low altitudes the structure of all four harmonic solutions is the same. Their differences occur only at high altitudes where E_L progressively develops smaller parallel structure as the harmonic number increases. According to the above analysis of the ratio $v_{g\perp}/v_{g\parallel}$, it may be concluded that at low altitudes, small transverse scale Alfvén waves at different harmonics are affected in the same manner by the inertial dispersion, but at high altitudes the higher-harmonic waves are more strongly affected by the kinetic dispersion. This difference in behavior of the different harmonic dispersive Alfvén waves originates from the parallel inhomogeneity of the plasma density and geomagnetic field, with a significant distinction between the fundamental FLR and higher odd harmonic FLRs.

This behavior of higher-harmonic FLRs suggests that under normal magnetospheric conditions, they would

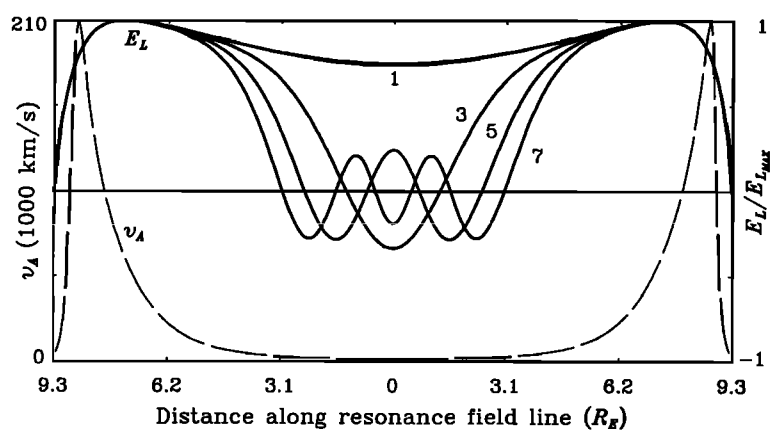

Figure 6. Distribution of the background v_A along the resonance field line (dashed curve) and corresponding profiles of E_L for the first four odd harmonics (solid curves), obtained by solving eigenvalue equation (24).

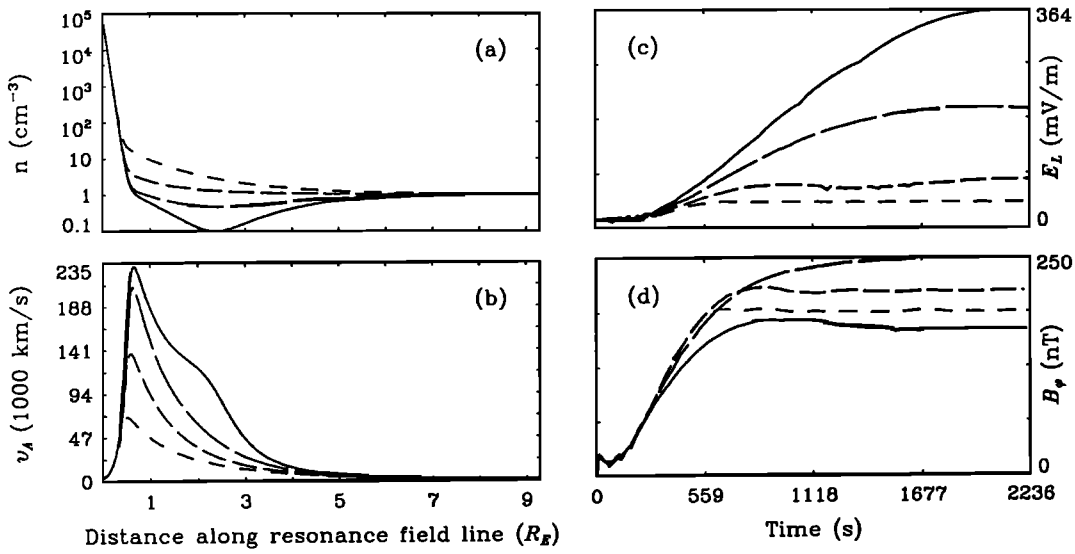

Figure 7. (a) Distributions of the background n_0 along the resonance field line. (b) Profiles of the corresponding v_A. (c) Evolution in time of E_L in fundamental FLRs. (d) Evolution in time of corresponding B_φ.

tend to produce multiple auroral forms [*Trondsen et al.*, 1997], rather than a single, discrete arc at high magnetic L shells. Otherwise, nonradiative harmonic FLRs can be expected mostly on lower magnetic shells, where the plasma is colder and inertial dispersion dominates over larger portion of the flux tube.

Computations of the model with hot magnetospheric ions show that even fundamental FLR radiates kinetic Alfvén waves on $L = 7.5$ unless the background plasma is not depleted at the lower magnetosphere. Figure 7a shows four profiles of n_0 along a resonance field line. The background density at radial distance 3 R_E is set equal to 0.1 cm^{-3} (solid curve), 0.5 cm^{-3} (long-dashed curve), 1.4 cm^{-3} (medium-dashed curve), and 3.6 cm^{-3} (short-dashed curve). Four profiles of the corresponding v_A are shown in Figure 7b. In spite of the fact that the maximum of v_A in these four cases changes more than 3 times, the difference in the corresponding fundamental eigenfrequencies is less than 3.5%. Figure 7c shows the temporal behavior of the maximum amplitude of E_L in four fundamental FLRs, and Figure 7d shows the temporal behavior of the maximum amplitude of the corresponding B_φ. The investigations reveal that the fundamental FLR on $L = 7.5$, with $T_{e*} = 150$ eV and $T_{i*} = 500$ eV, becomes nonradiative, when n_0 at the geocentric distance ≈ 3 R_E is in the range 0.1–0.5 cm^{-3}. Such a depletion of the background plasma density (auroral plasma cavity) is typically observed in the nightside auroral zone at that geocentric distance [*Persoon et al.*, 1988].

The occurrence of an auroral plasma cavity also affects small-scale, dispersive FLRs in two other ways. First, it increases the parallel potential drop between ionosphere and ≈ 4 R_E altitude by changing the distribution and amplitude of E_μ along the resonant field line. Thus in the computations with $n_{0_{\min}} = 0.5$ cm^{-3} the maximum parallel potential drop is equal to 1.02 kV. For the case when $n_{0_{\min}} = 0.1$ cm^{-3}, the same boundary generator produces a FLR with maximum parallel potential drop of 2.15 kV.

Second, because the inertial Alfvén waves satisfy the impedance relation $|E_L|/|B_\varphi| = v_A(1+k_\perp^2\lambda^2)^{1/2}$ [*Lysak and Dum*, 1983] and because a depletion in n_0 increases v_A and λ^2 at the same time, it is reasonable to expect that an auroral plasma cavity will cause the local ratio $|E_L|/|B_\varphi|$ to increase. Indeed, in the computations with $n_{0_{\min}} = 0.5$ cm^{-3}, a dispersive Alfvén wave with $E_L = 100$ mV/m at an altitude ≈ 1.74 R_E (where E_L has a maximum) has $B_\varphi = 36$ nT. For a case with $n_{0_{\min}} = 0.1$ cm^{-3}, a dispersive Alfvén wave with $E_L = 100$ mV/m at an altitude ≈ 2.3 R_E (where E_L has a maximum) has $B_\varphi = 8$ nT.

The last point of interest concerns the "thickness" and temporal evolution of the discrete auroral arc that may be produced by the parallel electric field of a nonradiative fundamental FLR. To connect the numerical results with optical ground-based observations of aurora, like that given by *Trondsen et al.* [1997], the negative parallel potential drop (which should accelerate electrons into the ionosphere) calculated from the nonradiative fundamental FLR along the dipole magnetic field lines and mapped to 100 km altitude, is used as a proxy for auroral luminosity. Results of this mapping are shown in the 11 curves of Figure 8. Each successive plot is a step in time of 1/10 of the wave period (≈ 88 s), and the entire sequence covers one full period of the process. The characteristic scale size of the "brightest" discrete arc (about time 35.2–44.0 s) in the north-south direction, measured as the width of the peak at half amplitude, is about 800 m. A further decrease of the north-south scale of this structure is limited by the spatial resolution of the code.

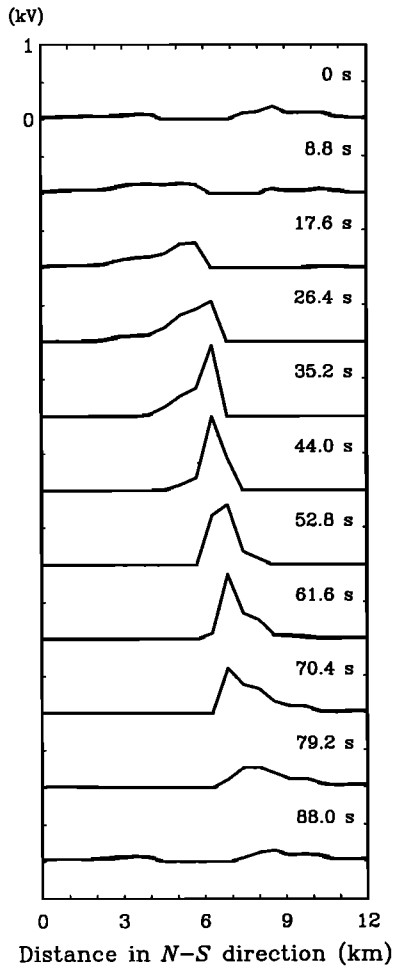

Figure 8. Projections of the negative parallel potential drop produced by the dispersive nonradiative fundamental FLR between the ionosphere and $\approx 4\ R_E$ altitude to 100 km altitude.

5. Conclusions

Results from the studies of small-scale, dispersive, nonradiative FLRs, including finite ion Larmor radius correction, can be summarized as follows:

1. A new MHD/kinetic model including finite ion Larmor radius effects and the wave relativistic correction (finite v_A/c) has been developed in dipole magnetic geometry to investigate the microstructure and temporal behavior of small-scale, dispersive Alfvén waves in the Earth's magnetosphere. The model is suitable for describing magnetically incompressible ULF waves with transverse scale sizes comparable to the ion Larmor radius.

2. The model reveals that hot magnetospheric ions significantly reduce the parallel electric field of ion Larmor scale dispersive Alfvén waves, with an expected reduction in the electron Landau damping of these waves in the magnetosphere. This conclusion is important when the propagation of a small-scale dispersive Alfvén wave along a high-latitude magnetic L shell threading hot magnetospheric plasma is considered.

3. If the parameters of the background plasma and magnetic field satisfy the condition $\rho^2 \approx \lambda^2$ (the transition region where inertial and kinetic dispersion effectively cancel each other), ion gyroscale dispersive Alfvén waves exhibit several novel properties, namely, they propagate exactly along magnetic field lines, satisfy the dispersion relation of the classical one-fluid MHD Alfvén wave, and carry parallel electric field.

4. Computations show that for realistic parameters of the background plasma and magnetic field the fundamental FLR can become nonradiative on auroral field lines near $L = 7.5$. In the absence of dissipation, fundamental nonradiative FLR can produce dispersive Alfvén waves with transverse scales less than 1 km at 100 km altitude. The parallel electric field of the small-scale Alfvén wave can produce a kV potential drop along the resonance field line between the ionosphere and $\approx 4\ R_E$ altitude.

5. A plasma density depletion in the lower auroral magnetosphere (auroral plasma cavity at $\approx$ 2–5 R_E geocentric distance) enables the formation of a nonradiative fundamental FLR. It also increases the net parallel potential drop and the ratio $|E_\perp|/|B_\perp|$ of small-scale, dispersive FLRs. The last fact may be important for the analysis of small-scale electromagnetic structures observed below 4 R_E altitude.

6. Owing to the parallel inhomogeneity of the background plasma density and geomagnetic field, higher-harmonic dispersive FLRs are more radiative in the equatorial magnetosphere than the fundamental mode.

Appendix: Elliptic Equations

In the computations presented in this paper, $A_\parallel$ and ϕ are defined at each time step as a numerical solution of the one-dimensional elliptic equations:

$$n_0 A_\parallel - \delta \nabla_L^2 A_\parallel = \mathcal{F} \tag{A1}$$

$$\nabla \cdot \left(1/v_A^2 + 1/c^2\right) \nabla_L \phi = \mathcal{G} \tag{A2}$$

with corresponding boundary conditions. Here $\mathcal{F}$ and $\mathcal{G}$ denote known right-hand parts, which are calculated using information from the previous time steps.

Equations (A1) and (A2) can be approximated at each interior grid point $(L_i,\ \mu_j)$ of the computational domain by the difference equation

$$-\, a_{i,j}\mathcal{A}_{i-1,j} + b_{i,j}\mathcal{A}_{i,j} - c_{i,j}\mathcal{A}_{i+1,j} = \mathcal{R}_{i,j} \tag{A3}$$

where $\mathcal{A}_{i,j}$ is the difference approximation of either $A_\parallel$ or ϕ; $\mathcal{R}_{i,j}$ is the difference approximation of the corresponding right-hand parts $\mathcal{F}$ or $\mathcal{G}$; and a, b, and c are numerical coefficients describing background media. Applying central difference formulas [*Burden and Faires*, 1989] to (A1), these coefficients can be obtained in the form

$$a_{i,j} = H_{i,j} \left(\frac{h_\varphi}{h_l h_\mu}\right)_{i-1/2,j} h_{\mu_{i-1,j}}$$

$$c_{i,j} = H_{i,j} \left(\frac{h_\varphi}{h_l h_\mu}\right)_{i+1/2,j} h_{\mu_{i+1,j}}$$

$$b_{i,j} = n_{0i,j} + H_{i,j}\left[\left(\frac{h_\varphi}{h_l h_\mu}\right)_{i-1/2,j} + \left(\frac{h_\varphi}{h_l h_\mu}\right)_{i+1/2,j}\right] h_{\mu i,j}$$

Here the subscript $i = 1, \ldots, 149$ denotes grids points with $L_i = 7.25 + iH_L$; the subscript $j = 1, \ldots, 100$ denotes grids points with μ_j corresponding to the distance $(j - 1/2)\,\mathcal{L}/100$ along the resonant field line ($L = 7.5$) from the southern ionosphere (320 km altitude); $\mathcal{L} = 18.6\ R_E$ is the total length of the resonant field line; $H_L = (7.75-7.25)/150$; and $H_{i,j} = (\delta/H_L^2)(1/h_L h_\varphi)_{i,j}$.

By analogy with the above forms, coefficients in the discrete approximation (A3) of (A2) can be obtained in the form

$$a_{i,j} = -H_{i,j}\left[\left(\frac{1}{v_A^2} + \frac{1}{c^2}\right)\frac{h_\varphi h_\mu}{h_L}\right]_{i-1/2,j}$$

$$c_{i,j} = -H_{i,j}\left[\left(\frac{1}{v_A^2} + \frac{1}{c^2}\right)\frac{h_\varphi h_\mu}{h_L}\right]_{i+1/2,j}$$

$$b_{i,j} = -a_{i,j} - c_{i,j}$$

Here the subscript i is the same as above and the subscript $j = 1, \ldots, 99$ denotes grid points with μ_j corresponding to the distance $j\,\mathcal{L}/100$ along the resonant field line from the southern ionosphere.

In inhomogeneous media, coefficients a, b, and c depend on space but do not depend on time. So all of them are calculated only once at the beginning of the computation and used repeatedly after that.

Approximation (A3) together with lateral boundary conditions leads each (A1) and (A2) to a linear algebraic system of 149 equations defining $A_\parallel$ and ϕ. Structurally, these systems have a tridiagonal matrix which can be inverted numerically by a number of well-known techniques. In our numerical code the so-called Thomas algorithm [*Strikwerda*, 1989] is successfully used.

Acknowledgments. The research was supported in part at Dartmouth by NASA under grants NAG5-2252, NAG5-1098, and NAG5-4529, and at PPPL by NSF grant ATM-9523331 and DOE contract DE-AC02-76-CH3073.

The Editor thanks Daniel W. Swift and Robert Rankin for their assistance in evaluating this paper.

References

Aikio, A. T., G. T. Marklund. J. Woch, and T. A. Potemra, Small-scale structures in the high-altitude auroral electric field, *Ann. Geophys.*, *13*, 84, 1995.

Anderson, B. J., M. J. Engebretson, S. P. Rounds, L. J. Zanetti, and T. A. Potemra, A statistical study of Pc 3-5 pulsations observed by the AMPTE/CCE magnetic field experiment, 1, Occurrence distributions, *J. Geophys. Res.*, *85*, 10,495, 1990.

Bennett, E. L., M. Temerin, and F. S. Mozer, The distribution of auroral electrostatic shocks below 8000-km altitude, *J. Geophys. Res.*, *88*, 7107, 1983.

Boehm, M. H., C. W. Carlson, J. P. McFadden, J. H. Clemmons, and F. S. Mozer, High-resolution sounding rocket observations of large-amplitude Alfvén waves, *J. Geophys. Res.*, *95*, 12,157, 1990.

Borovsky, J. E., Auroral arc thicknesses as predicted by various theories, *J. Geophys. Res.*, *98*, 6101, 1993.

Burden, R. L., and J. D. Faires, *Numerical Analysis*, 729 pp., PWS-KENT, Boston, Mass., 1989.

Chen, L., and A. Hasegawa, A theory of long-period magnetic pulsations, 1, Steady state excitation of field line resonance, *J. Geophys. Res.*, *79*, 1024, 1974.

Cheng, C. Z., A kinetic-magnetohydrodynamic model for low-frequency phenomena, *J. Geophys. Res.*, *96*, 21,159, 1991.

Cheng, C. Z., T. C. Chang, C. A. Lin, and W. H. Tsai, Magnetohydrodynamic theory of field line resonances in the magnetosphere, *J. Geophys. Res.*, *98*, 11,339, 1993.

Chmyrev, V. M., S. V. Bilichenko, O. A. Pokhotelov, V. A. Marchenko, V. I. Lazarev, A. V. Streltsov, and L. Stenflo, Alfvén vortices and related phenomena in the ionosphere and the magnetosphere, *Phys. Scr.*, *38*, 841, 1988.

Chmyrev, V. M., V. A. Marchenko, O. A. Pokhotelov, P. K. Shukla, L. Stenflo, and A. V. Streltsov, The development of discrete active auroral forms, *IEEE Trans. Plasma Sci.*, *20*, 764, 1992.

Cummings, W. D., R. J. O'Sullivan, and P. J. Coleman Jr., Standing Alfvén waves in the magnetosphere, *J. Geophys. Res.*, *74*, 778, 1969.

Davis, N. T., Observed characteristics of auroral forms, *Space Sci. Rev.*, *22*, 77, 1978.

Dubinin, E. M., P. I. Israelevich, N. S. Nikolaeva, I. Kutiev, and I. M. Podgorny, Localized auroral disturbance in the morning sector of topside ionosphere as a standing electromagnetic wave, *Planet. Space Sci.*, *33*, 597, 1985.

Goertz, C. K., Kinetic Alfvén waves on auroral field lines, *Planet. Space Sci.*, *32*, 1387, 1984.

Goertz, C. K., and R. W. Boswell, Magnetosphere-ionosphere coupling, *J. Geophys. Res.*, *84*, 7239, 1979.

Greenwald, R. A., and A. D. M. Walker, Energetics of long period resonant hydromagnetic waves, *Geophys. Res. Lett.*, *7*, 745, 1980.

Haerendel, G., An Alfvén wave model of auroral arcs, in *High-Latitude Space Plasma Physics*, edited by B. Hultqvist and T. Hagfors, pp. 515-535, Plenum, New York, 1983.

Hasegawa, A., Particle acceleration by MHD surface wave and formation of aurora, *J. Geophys. Res.*, *81*, 5083, 1976.

Hasegawa, A., and C. Uberoi, *The Alfvén Wave*, 128 pp., U.S. Dep. of Energy, Washington, D. C., 1982.

Hazeltine, R. D., and J. D. Meiss, Shear-Alfvén dynamics of toroidally confined plasmas, *Phys. Rep.*, *121*, pp. 1–164, 1985.

Hazeltine, R. D., C. T. Hsu, and P. J. Morrison, Hamiltonian four-field model for nonlinear tokamak dynamics, *Phys. Fluids*, *30*, 3204, 1987.

Hughes, W. J., and R. J. L. Gerard, A second harmonic geomagnetic field line resonance at the inner edge of the plasma sheet: GOES 1, ISEE 1, and ISEE 2 observations, *J. Geophys. Res.*, *89*, 2755, 1984.

Hughes, W. J., and D. J. Southwood, The screening of micropulsation signals by the atmosphere and ionosphere, *J. Geophys. Res.*, *81*, 3234, 1976.

Hui, C.-H., and C. E. Seyler, Electron acceleration by Alfvén waves in the magnetosphere, *J. Geophys. Res.*, *97*, 3953, 1992.

Inhester, B., Numerical modeling of hydromagnetic wave coupling in the magnetosphere, *J. Geophys. Res.*, *92*, 4751, 1987.

Johnson, J. R., and C. Z. Cheng, Kinetic Alfvén waves and plasma transport at the magnetopause, *Geophys. Res. Lett.*, *24*, 1423, 1997.

Kadomtsev, B. B., *Plasma Turbulence*, Academic, San Diego, Calif., 1965.

Karlsson, T., and G. T. Marklund, A statistical study of intense low-altitude electric fields observed by Freja, *Geophys. Res. Lett.*, *23*, 1005, 1996.

Kletzing, C., C. Cattell, F. S. Mozer, S.-I. Akasofu, and K.

Makita, Evidence for electrostatic shocks as the source of discrete auroral arcs, *J. Geophys. Res.*, *88*, 4105, 1983.

Kletzing, C A., Electron acceleration by kinetic Alfvén waves, *J. Geophys. Res.*, *99*, 11,095, 1994.

Kouznetsov, I., and W. Lotko, Radial energy transport by magnetospheric ULF waves: Effects of magnetic curvature and plasma pressure, *J. Geophys. Res.*, *100*, 7599, 1995.

Lysak, R. L., and C. W. Carlson, Effect of microscopic turbulence on magnetosphere-ionosphere coupling, *Geophys. Res. Lett.*, *8*, 269, 1981.

Lysak, R. L., and C. T. Dum, Dynamics of magnetosphere-ionosphere coupling including turbulent transport, *J. Geophys. Res.*, *88*, 365, 1983.

Lysak, R. L., and W. Lotko, On the kinetic dispersion relation for shear Alfvén waves, *J. Geophys. Res.*, *101*, 5085, 1996.

Mallinckrodt, A. J., and C. W. Carlson, Relations between transverse electric fields and field-aligned currents, *J. Geophys. Res.*, *83*, 1426, 1978.

Marklund, G., L. Blomberg, C.-G. Falthammar, P.-A. Lindqvist, and L. Eliasson, On the occurrence and characteristics of intense low-altitude electric fields, *Ann. Geophys.*, *13*, 704, 1995.

McFadden, J. P., C. W. Carlson, and M. H. Boehm, Field-aligned electron precipitation at the edge of an arc, *J. Geophys. Res.*, *91*, 1723, 1986.

Mishin, E. V., and M. Förster, "Alfvénic shocks" and low-altitude auroral acceleration, *Geophys. Res. Lett.*, *22*, 1745, 1995.

Moore, T. E., D. L. Gallagher, J. L. Horwitz, and R. H. Comfort, MHD wave breaking in the outer plasmasphere, *Geophys. Res. Lett.*, *14*, 1007, 1987.

Morrison, P. J., and J. M. Green, Noncanonical Hamiltonian density formulation of hydrodynamics and ideal magnetohydrodynamics, *Phys. Rev. Lett.*, *45*, 790, 1980.

Morrison, P. J., and R. D. Hazeltine, Hamiltonian formulation of reduced magnetohydrodynamics, *Phys. Fluids*, *27*, 886, 1984.

Mozer, F. S., ISEE-1 observations of electrostatic shocks on auroral zone field lines between 2.5 and 7 Earth radii, *Geophys. Res. Lett.*, *8*, 823, 1981.

Persoon, A. M., D. A. Gurnett, W. K. Peterson, J. H. Waite Jr., J. L. Burch, and J. L. Green, Electron density depletions in the nightside auroral zone, *J. Geophys. Res.*, *93*, 1871, 1988.

Radoski, H. R., A note on oscillating field lines, *J. Geophys. Res.*, *72*, 418, 1967.

Rankin, R., B. G. Harold, J. C. Samson, and P. Frycz, The nonlinear evolution of field line resonances in the Earth's magnetosphere, *J. Geophys. Res.*, *98*, 5839, 1993.

Rankin, R., P. Frycz, V. T. Tikhonchuk, and J. C. Samson, Ponderomotive saturation of magnetospheric field line resonances, *Geophys. Res. Lett.*, *22*, 1741, 1995.

Samson, J. C., T. J. Hughes, F. Creutzberg, D. D. Wallis, R. A. Greenwald, and J. M. Ruohoniemi, Observations of detached, discrete arc in association with field line resonances, *J. Geophys. Res.*, *96*, 15,683, 1991.

Samson, J. C., D. D. Wallis, T. J. Hughes, F. Greutzberg, J. M. Ruohoniemi, and R. A. Greenwald, Substorm intensifications and field line resonances in the nightside magnetosphere, *J. Geophys. Res.*, *97*, 8495, 1992.

Samson, J. C., L. L. Cogger, and Q. Pao, Observations of field line resonances, auroral arcs, and auroral vortex structures, *J. Geophys. Res.*, *101*, 17,373, 1996.

Seyler, C. E., Nonlinear 3-D evolution of bounded kinetic Alfvén waves due to shear flow and collisionless tearing instability, *Geophys. Res. Lett.*, *15*, 756, 1988.

Seyler, C. E., A mathematical model of the structure and evolution of small-scale discrete auroral arcs, *J. Geophys. Res.*, *95*, 17,199, 1990.

Southwood, D. J., Some features of field line resonances in the magnetosphere, *Planet. Space Sci.*, *22*, 483, 1974.

Spiro, R. W., P. H. Reiff, and L. J. Maher, Precipitating electron energy flux and auroral zone conductances: An empirical model, *J. Geophys. Res.*, *87*, 8215, 1982.

Strauss, H. R., Nonlinear, three-dimensional magnetohydrodynamics of noncircular tokamaks, *Phys. Fluids*, *19*, 134, 1976.

Streltsov, A. V., and W. Lotko, Dispersive field line resonances on auroral field lines, *J. Geophys. Res.*, *100*, 19,457, 1995.

Streltsov, A. V., and W. Lotko, The fine structure of dispersive, nonradiative field line resonance layers, *J. Geophys. Res.*, *101*, 5343, 1996.

Streltsov, A. V., and W. Lotko, Dispersive, nonradiative field line resonances in a dipolar magnetic field geometry, *J. Geophys. Res.*, *102*, 27,121, 1997.

Strikwerda, J. C., *Finite Difference Schemes and Partial Differential Equations*, 386 pp., Wadsworth, Belmont, Calif., 1989.

Swift, D. W., On the formation of auroral arcs and the acceleration of auroral electrons, *J. Geophys. Res.*, *80*, 2096, 1975.

Temerin, M., J. McFadden, M. Boehm, C. W. Carlson, and W. Lotko, Production of flickering aurora and field-aligned electron flux by electromagnetic ion cyclotron waves, *J. Geophys. Res.*, *91*, 5769, 1986.

Trondsen, T. S., L. L. Cogger, and J. C. Samson, Asymmetric multiple auroral arcs and inertial Alfvén waves, *Geophys. Res. Lett.*, *24*, 2945, 1997.

Vickrey, J. F., R. R. Vondrak, and S. J. Matthews, The diurnal and latitudinal variations of auroral-zone ionospheric conductivity, *J. Geophys. Res.*, *86*, 65, 1981.

Wei, C. Q., J. C. Samson, R. Rankin, and P. Frycz, Electron inertial effects on geomagnetic field line resonances, *J. Geophys. Res.*, *99*, 11,265, 1994.

Weimer, D. R., and D. A. Gurnett, Large-amplitude auroral electric fields measured with DE-1, *J. Geophys. Res.*, *98*, 13,557, 1993.

Xu, B.-L., J. C. Samson, W. W. Liu, F. Creutzberg, and T. J. Hughes, Observations of optical aurora modulated by resonant Alfvén waves, *J. Geophys. Res.*, *98*, 11,531, 1993.

Zhu, X., and M. G. Kivelson, Compressional ULF waves in the outer magnetosphere, 1, Statistical study, *J. Geophys. Res.*, *96*, 19,451, 1991.

C. Z. Cheng and J. R. Johnson, Plasma Physics Laboratory, Princeton University, Princeton, NJ 08543. (fcheng@pppl.gov; jrj@pppl.gov)

W. Lotko and A. V. Streltsov, Thayer School of Engineering, Dartmouth College, 8000 Cummings Hall, Hanover, NH 03755-8000. (billl@cyberia.dartmouth.edu; as@exos.dartmouth.edu)

(Received January 30, 1998; revised August 10, 1998; accepted August 12, 1998.)